Nanotechnology **21** (2010) 085708 (9pp) doi:10.1088/0957-4484/21/8/085708

Mechanics of nanowire/nanotube in-surface buckling on elastomeric substrates

J Xiao[1], S Y Ryu[2], Y Huang[1,3], K-C Hwang[4], U Paik[2] and J A Rogers[5]

[1] Department of Mechanical Engineering, Northwestern University, Evanston, IL 60208, USA
[2] Division of Materials Science and Engineering, Hanyang University, 17 Hangdang-dong, Sungdong-gu, Seoul 133-791, Republic of Korea
[3] Department of Civil and Environmental Engineering, Northwestern University, Evanston, IL 60208, USA
[4] Department of Engineering Mechanics, Tsinghua University, Beijing 100084, People's Republic of China
[5] Department of Materials Science and Engineering, Frederick-Seitz Materials Research Laboratory and Beckman Institute, University of Illinois at Urbana-Champaign, Illinois 61801, USA

E-mail: y-huang@northwestern.edu and jrogers@uiuc.edu

Received 10 August 2009, in final form 21 December 2009
Published 25 January 2010
Online at stacks.iop.org/Nano/21/085708

Abstract
A continuum mechanics theory is established for the in-surface buckling of one-dimensional nanomaterials on compliant substrates, such as silicon nanowires on elastomeric substrates observed in experiments. Simple analytical expressions are obtained for the buckling wavelength, amplitude and critical buckling strain in terms of the bending and tension stiffness of the nanomaterial and the substrate elastic properties. The analysis is applied to silicon nanowires, single-walled carbon nanotubes, multi-walled carbon nanotubes, and carbon nanotube bundles. For silicon nanowires, the measured buckling wavelength gives Young's modulus to be 140 GPa, which agrees well with the prior experimental studies. It is shown that the energy for in-surface buckling is lower than that for normal (out-of-surface) buckling, and is therefore energetically favorable.

(Some figures in this article are in colour only in the electronic version)

1. Introduction

Buckling of thin layers or aligned arrays of stiff materials on elastomeric substrates has many important applications, such as stretchable electronics [1–11], precision metrology [12–14] and flexible optoelectronics [15]. These systems show normal buckling, i.e., the stiff thin layers buckle normal to the substrate surface. Their mechanics is well understood [16–24]. By contrast, Ryu *et al* [25] recently reported for the first time that silicon nanowires (SiNWs) on elastomeric substrates buckle only within the substrate surface, i.e. in-surface buckling. Figure 1(a) summarizes the experimental process used in this case. SiNWs were first prepared on Si substrates using Au nanoclusters as catalysts in a vapor–liquid–solid (VLS) process. Each nanocluster served as a site that directs preferential addition of the reactant to the end of a growing SiNW. Next, the randomly oriented SiNWs formed in this way were transferred, using shear force, to another silicon wafer substrate to form aligned arrays (figure 1(a), top frame) [26–28]. These arrays were then transferred to a prestrained PDMS substrate (uniaxially tensile along the lengths of the SiNWs) [29–32]. After releasing the prestrain, the resulting collection of buckled SiNWs (figure 1(a), bottom frame) was examined by atomic force microscope (AFM) and field-emission scanning electron microscope (FE-SEM) images. Figure 1(b) shows some representative results.

The purpose of this paper is to provide detailed mechanics analysis of in-surface buckling of one-dimensional

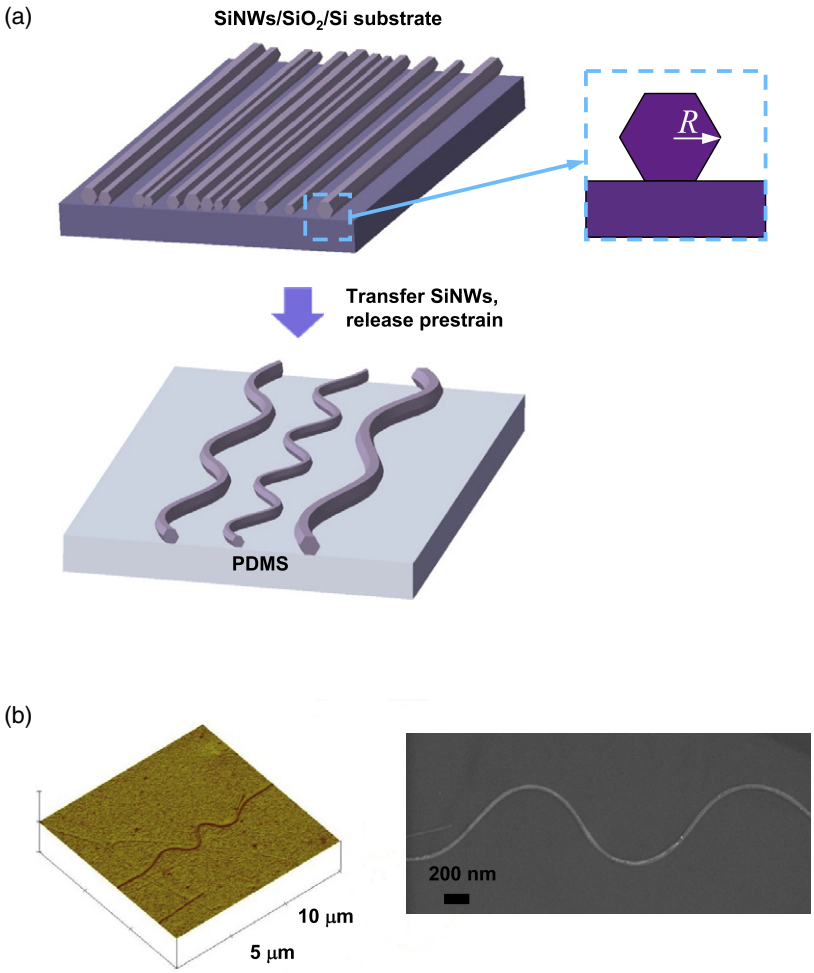

Figure 1. (a) Schematic diagram of the process to form laterally (in-surface) buckled, wavy SiNWs on PDMS substrates. (b) AFM (left) and FE-SEM (right) images of laterally buckled SiNWs on PDMS substrates.

nanomaterials (e.g., nanowires, nanotubes) on elastomeric substrates. Similar to normal buckling [33], in-surface buckling may occur when nanowires and nanotubes are sufficiently thin (e.g., <100 nm). For pure elastic deformation, mechanics analysis can be applied down to ∼10 atomic spacing [34, 35], i.e., when the characteristic length of deformation is as small as ∼10 atomic spacings, which correspond to 2 and 0.5 nm radii for SiNWs and carbon nanotubes, respectively. Similar to the study of normal buckling of stiff thin films and single-walled carbon nanotubes (SWNTs) on compliant substrates [16, 19–24], the mechanics analysis for in-surface buckling in section 2 gives analytically the total energy of the system, which consists of the bending energy U_b and membrane energy U_m in the stiff beam, and strain energy U_S in the substrate. The buckling wavelength and amplitude are then obtained analytically by minimizing the total energy. This is applied to SiNWs, SWNTs, multi-walled carbon nanotubes (MWNTs), and carbon nanotube bundles in sections 3–6, respectively. These systems may find various applications [36–39] since SiNWs and carbon nanotubes have superior and unique properties [40–45].

As to be shown in sections 3–6, in-surface buckling gives lower total energy than normal buckling for SiNWs, SWNTs, MWNTs and carbon nanotube bundles, and is therefore energetically favorable. This explains the experimentally observed in-surface buckling of SiNWs [25], but not normal buckling of SWNTs [14]. The latter is because the SWNT radius (∼1 nm) is comparable to or even smaller than the roughness of the PDMS surface (∼1 nm), which prevents in-surface buckling of SWNTs. The surface roughness, however, is much smaller than the radius of SiNWs (∼50 nm), and therefore cannot prevent in-surface buckling.

2. Mechanics of in-surface buckling of stiff beams on a compliant substrate

Let EI and EA denote the bending and tension stiffness of a stiff beam on the surface of a compliant substrate, respectively. The lateral deflection v within the substrate surface of the buckled beam can be described by a sinusoidal form $v = v_{max} \cos kx$, where the coordinate x is along the beam axis, v_{max} is the buckling amplitude, and the wavevector k is related to the wavelength λ by $k = 2\pi/\lambda$. The bending energy per

unit length of the buckled beam is obtained as

$$U_{\rm b} = \frac{1}{\lambda}\int_0^{\lambda}\frac{1}{2}EI\left(\frac{{\rm d}^2 v}{{\rm d}x^2}\right)^2 {\rm d}x = \frac{EI}{4}v_{\rm max}^2 k^4. \qquad (1)$$

The membrane strain in the beam is given in terms of the lateral deflection v and axial displacement u by $\varepsilon_{\rm m} = {\rm d}u/{\rm d}x + ({\rm d}v/{\rm d}x)^2/2$. The shear stress at the beam/substrate interface is negligible since Young's modulus for the beam (e.g., ~140 GPa for SiNWs and 1.25 TPa for SWNTs) [14, 25] is several orders of magnitude larger than that for the substrate (e.g., ~2 MPa at room temperature) [46]. Force equilibrium then requires a constant membrane force (and a constant membrane strain) in the buckled beam, which gives the axial displacement $u = kv_{\rm max}^2 \sin(2kx)/8 - \varepsilon_{\rm pre}x$, where $-\varepsilon_{\rm pre}$ is the compressive strain in the beam due to the relaxation of prestrain applied to the substrate. The membrane strain is $\varepsilon_{\rm m} = k^2 v_{\rm max}^2/4 - \varepsilon_{\rm pre}$, which then gives the membrane energy in the beam

$$U_{\rm m} = \frac{1}{\lambda}\int_0^{\lambda}\frac{1}{2}EA\varepsilon_{\rm m}^2\,{\rm d}x = \frac{EA}{2}\left(\frac{k^2 v_{\rm max}^2}{4} - \varepsilon_{\rm pre}\right)^2. \qquad (2)$$

The lateral force (per unit length) on the beam due to buckling, which is needed to calculate the energy in the substrate next, is obtained from beam theory [47] as $T = EI{\rm d}^4 v/{\rm d}x^4 - EA\varepsilon_{\rm m}{\rm d}^2 v/{\rm d}x^2 = -P\cos kx$, where $P = -EAv_{\rm max}k^2(k^2 v_{\rm max}^2/4 - \varepsilon_{\rm pre}) - EIv_{\rm max}k^4$.

The substrate is modeled as a semi-infinite solid since its thickness is much larger than the buckling wavelength of the beams. Let $E_{\rm S}$ denote Young's modulus for the poly(dimethylsiloxane) (PDMS) substrate in figure 1, and $\nu_{\rm S}$ Poisson's ratio. The substrate surface is traction-free except for the stripe underneath the beam, which has width $2w$ and is along the x direction. The shear stress traction in this region due to beam buckling is the average of the lateral force $P\cos kx$ over the width, i.e., $P\cos kx/(2w)$. For a point (x, y) on the substrate surface (x is along the beam axis), the lateral displacement (along the y direction) induced by a unit lateral point force (also along the y direction) at (ξ, ψ) on the surface of the semi-infinite solid is given by $[(1-\nu_{\rm S})(x-\xi)^2 + (y-\psi)^2]/[(1-\nu_{\rm S})\pi\bar{E}_{\rm S}\rho^3]$ [48], where $\bar{E}_{\rm S} = E_{\rm S}/(1-\nu_{\rm S}^2)$ is the plane-strain modulus of the substrate, and $\rho = \sqrt{(x-\xi)^2 + (y-\psi)^2}$. For the lateral stress traction $P\cos kx/(2w)$ over the width $2w$, the lateral displacement (along the y direction) on the surface can be obtained by integrating the above function as $v_{\rm sub} = P\cos kx\int_{-w}^{w}[(1-\nu_{\rm S})K_0(k|y-\psi|) + \nu_{\rm S}k|y-\psi|K_1(k|y-\psi|)]\,{\rm d}\psi/[\pi\bar{E}_{\rm S}w(1-\nu_{\rm S})]$, where K_0 and K_1 are modified Bessel functions of the second kind [49]. For the buckling wavelength much larger than the width (i.e., $kw \ll 1$), the modified Bessel functions can be approximated by their asymptotic expansions, $K_0(k|y-\psi|) \approx -\ln(k|y-\psi|/2) - \gamma$ and $K_1(k|y-\psi|) = 1/(k|y-\psi|)$, where $\gamma = 0.577$ is Euler's constant [49]. The lateral displacement (along the y direction) on the surface then becomes $v_{\rm sub} = P\cos kx\{2w[(1-\nu_{\rm S})^{-1} + \ln 2 - \gamma] - (w+y)\ln(k|w+y|) - (w-y)\ln(k|w-y|)\}/(\pi\bar{E}_{\rm S}w)$. The strain energy in the substrate (per unit length) is obtained via the divergence theorem as

$$U_{\rm S} = \frac{k}{2\pi}\int_0^{\frac{2\pi}{k}}\int_{-w}^{w}\frac{1}{2}\frac{P\cos(kx)}{2w}v_{\rm sub}\,{\rm d}y\,{\rm d}x = \frac{P^2}{4\pi\bar{E}_{\rm S}}\left(\frac{3-\nu_{\rm S}}{1-\nu_{\rm S}} - 2\gamma - 2\ln kw\right). \qquad (3)$$

The total potential energy $\Pi_{\rm tot}$ (per unit length) of the system is obtained as

$$\Pi_{\rm tot} = U_{\rm b} + U_{\rm m} + U_{\rm S} - \frac{1}{\lambda}\int_0^{\lambda}\int_{-w}^{w}\frac{P\cos kx}{2w} \times (v_{\rm sub} - v_{\rm max}\cos kx)\,{\rm d}x\,{\rm d}y = \frac{EI}{4}v_{\rm max}^2 k^4 + \frac{EA}{2}\left(\frac{k^2 v_{\rm max}^2}{4} - \varepsilon_{\rm pre}\right)^2 + \frac{1}{2}Pv_{\rm max} - \frac{P^2}{4\pi\bar{E}_{\rm S}}\left(\frac{3-\nu_{\rm S}}{1-\nu_{\rm S}} - 2\gamma - 2\ln kw\right), \qquad (4)$$

where the integration represents the work across the beam/substrate interface. The minimization of $\Pi_{\rm tot}$ with respect to $v_{\rm max}$ and k gives the following equations to determine the buckling wavevector and amplitude,

$$\left(\frac{EI}{\bar{E}_{\rm S}}\right)^{1/4} k = \left[\frac{2\pi\left(\frac{1}{1-\nu_{\rm S}} - \gamma - \ln kw\right)}{\left(\frac{3-\nu_{\rm S}}{1-\nu_{\rm S}} - 2\gamma - 2\ln kw\right)^2}\right]^{1/4}, \qquad (5)$$

$$v_{\rm max} = \frac{2}{k}\sqrt{\varepsilon_{\rm pre} - \varepsilon_{\rm c}}, \qquad (6)$$

where $\varepsilon_{\rm c} = \{EIk^4 + \pi\bar{E}_{\rm S}[(3-\nu_{\rm S})(1-\nu_{\rm S})^{-1} - 2\gamma - 2\ln kw]^{-1}\}/(EAk^2)$ is the critical buckling strain of a stiff beam on a compliant substrate. The beam buckles once the prestrain $\varepsilon_{\rm pre}$ reaches $\varepsilon_{\rm c}$, and the buckling amplitude then increases with the prestrain.

The right-hand side of equation (5) is essentially a constant because both logarithmic and one-fourth power functions change very slowly with kw. For a nearly incompressible substrate such as PDMS, $\nu_{\rm S} \approx 1/2$, this constant is approximately 5/7 (error on the order of 1%) such that the wavevector k and wavelength λ are given by

$$k = \frac{5}{7}\left(\frac{\bar{E}_{\rm S}}{EI}\right)^{1/4}, \qquad \lambda = \frac{14\pi}{5}\left(\frac{EI}{\bar{E}_{\rm S}}\right)^{1/4}. \qquad (7)$$

The wavelength is governed by the ratio of beam bending stiffness to substrate elastic modulus, and is independent of the prestrain $\varepsilon_{\rm pre}$. This provides experimentally simple routes to measure the linear elastic modulus of nanomaterials, including nanowires and nanotubes.

The bending stiffness EI of SiNW, SWNT, MWNT and carbon nanotube bundles is substituted into equations (6) and (7) to determine the buckling amplitude and wavelength for each nanomaterial in the following sections. In addition, the maximum strains in the buckled nanomaterials are also obtained.

3. In-surface buckling of silicon nanowires on a PDMS substrate

A SiNW has a hexagonal cross section with radius R, as shown in figure 1(a) [50]. Its moment of inertia and cross sectional area are $I_{\mathrm{SiNW}} = (5\sqrt{3}/16)R^4$ and $A_{\mathrm{SiNW}} = (3\sqrt{3}/2)R^2$, respectively. It has one side in contact with the substrate surface, thus the width of the contact region $2w_{\mathrm{SiNW}} = R$. The wavelength in equation (7) then becomes (<1% error)

$$\lambda_{\mathrm{SiNW}} = \frac{12\pi R}{5}\left(\frac{E_{\mathrm{SiNW}}}{\bar{E}_{\mathrm{S}}}\right)^{1/4}, \tag{8}$$

which is linearly proportional to the SiNW radius R, and to the 1/4 power of the SiNW to substrate moduli ratio. It is two orders of magnitude larger than the SiNW radius since E_{SiNW} is 5 orders of magnitude higher than the PDMS modulus, which justifies modeling SiNWs as beams. The buckling amplitude is obtained from equation (6) by substituting wavenumber k with $2\pi/\lambda_{\mathrm{SiNW}}$ as

$$(v_{\max})_{\mathrm{SiNW}} = \frac{12R}{5}\left(\frac{E_{\mathrm{SiNW}}}{\bar{E}_{\mathrm{S}}}\right)^{1/4}\sqrt{\varepsilon_{\mathrm{pre}} - (\varepsilon_{\mathrm{c}})_{\mathrm{SiNW}}} = \frac{\lambda_{\mathrm{SiNW}}}{\pi}\sqrt{\varepsilon_{\mathrm{pre}} - (\varepsilon_{\mathrm{c}})_{\mathrm{SiNW}}}, \tag{9}$$

which is linearly proportional to the buckling wavelength, and increases with the prestrain, where the critical buckling strain $(\varepsilon_{\mathrm{c}})_{\mathrm{SiNW}} \approx 0.3(\bar{E}_{\mathrm{S}}/E_{\mathrm{SiNW}})^{1/2}$.

Equation (8) can be rewritten as $E_{\mathrm{SiNW}} = \bar{E}_{\mathrm{S}}[5\lambda_{\mathrm{SiNW}}/(12\pi R)]^4$ to estimate Young's modulus for SiNW from the measured wavelengths and radii of buckled SiNWs. Detailed experimental procedures can be found in [25]. For the PDMS Young's modulus $E_{\mathrm{S}} = 2$ MPa (room temperature) [46] and Poisson's ratio $\nu_{\mathrm{S}} = 0.5$, figure 2(a) yields Young's modulus for SiNW $E_{\mathrm{SiNW}} = 140$ GPa, which agrees well with prior values reported for SiNW [51–53]. The buckling amplitude given by equation (8) also agrees well with experiments, as shown in figure 2(b), where the prestrain is 27% calculated from the measured contour length $\lambda_{\mathrm{contour}}$ and buckling wavelength λ via $\varepsilon_{\mathrm{pre}} = \ln(\lambda_{\mathrm{contour}}/\lambda)$ [21].

The maximum strain in SiNW is the sum of the membrane strain $\varepsilon_{\mathrm{m}} = k^2 v_{\max}^2/4 - \varepsilon_{\mathrm{pre}} = -(\varepsilon_{\mathrm{c}})_{\mathrm{SiNW}}$ and bending strain $\varepsilon_{\mathrm{b}} = (\mathrm{d}^2 v/\mathrm{d}x^2)R = -(5/3)\sqrt{(10/3)(\varepsilon_{\mathrm{c}})_{\mathrm{SiNW}}[\varepsilon_{\mathrm{pre}} - (\varepsilon_{\mathrm{c}})_{\mathrm{SiNW}}]}$. Its magnitude is

$$\varepsilon_{\max} = (\varepsilon_{\mathrm{c}})_{\mathrm{SiNW}} + \tfrac{5}{3}\sqrt{\tfrac{10}{3}(\varepsilon_{\mathrm{c}})_{\mathrm{SiNW}}[\varepsilon_{\mathrm{pre}} - (\varepsilon_{\mathrm{c}})_{\mathrm{SiNW}}]} \approx 3\sqrt{(\varepsilon_{\mathrm{c}})_{\mathrm{SiNW}}\varepsilon_{\mathrm{pre}}}, \tag{10}$$

because the critical buckling strain $(\varepsilon_{\mathrm{c}})_{\mathrm{SiNW}} \approx 0.3(\bar{E}_{\mathrm{S}}/E_{\mathrm{SiNW}})^{1/2}$ (0.13% for SiNWs on PDMS) is negligible as compared to the prestrain $\varepsilon_{\mathrm{pre}}$. For $\varepsilon_{\mathrm{pre}} = 5\%$, 10% and 27%, the maximum strain in SiNW is 2.6%, 3.6% and 5.9%, respectively, which is less than the yield strain (strength to modulus ratio) of 6.4% for SiNW [54].

Rather than normal buckling, SiNWs buckle within the surface of PDMS in the experiments because the in-surface buckling mode gives lower potential energy. For $\varepsilon_{\mathrm{pre}} = 27\%$ as in experiments, figure 2(c) shows that the potential energy for normal buckling [20] is larger than that in equation (4) for in-surface buckling, and their difference increases rapidly with the SiNW radius. This explains the experimentally observed in-surface buckling of SiNWs. For comparison, figure 2(c) also shows the adhesion energy (energy per unit length) between SiNWs and PDMS, which is the work of adhesion (energy

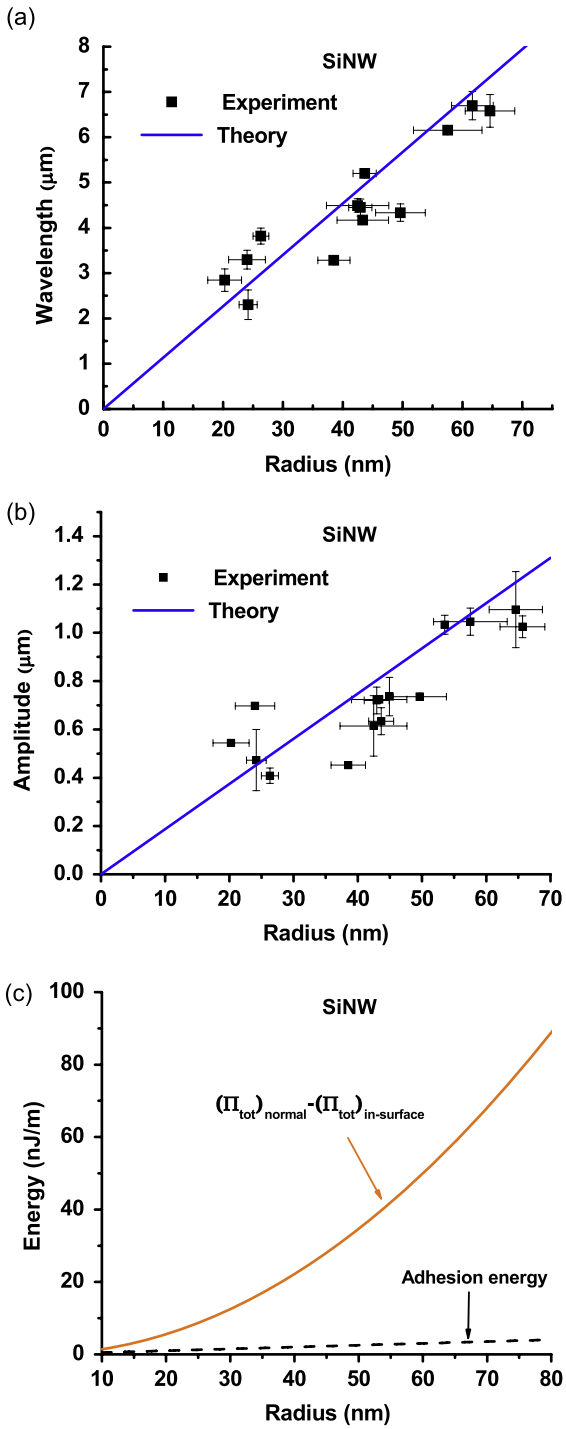

Figure 2. In-surface buckling of SiNWs on PDMS substrates. (a) Buckling wavelength versus SiNW radius. (b) Buckling amplitude versus SiNW radius. (c) Energy difference between normal and in-surface buckling, and the adhesion energy between SiNWs and PDMS, versus SiNW radius.

per unit area), 50.6 mJ m^{-2} [26], multiplied by the contact width. The energy difference between normal and in-surface buckling is much larger than the adhesion energy, particularly at relatively large radius.

4. In-surface buckling of single-walled carbon nanotubes on a PDMS substrate

A SWNT of radius R has the bending stiffness $E_{\rm CNT}I = \pi E_{\rm CNT}tR^3$ and tension stiffness $E_{\rm CNT}A = 2\pi E_{\rm CNT}tR$, where Young's modulus and the thickness of SWNT appear together, and $E_{\rm CNT}t = 0.42$ TPa nm [14]. The width $2w$ of the contact region between the SWNT and PDMS substrate is $2R$ [20]. By substituting the bending stiffness EI in equation (7) with that of SWNT $E_{\rm CNT}I = \pi E_{\rm CNT}tR^3$, the wavelength in equation (7) becomes

$$\lambda_{\rm SWNT} = \frac{14\pi}{5}\left(\frac{\pi E_{\rm CNT}tR^3}{\bar{E}_{\rm S}}\right)^{1/4}, \qquad (11)$$

which is about 5% larger than the wavelength for normal buckling of SWNTs [20]. The wavelength is proportional to $R^{3/4}$, and is shown in figure 3(a) for $E_{\rm S} = 2$ MPa and $\nu_{\rm S} = 0.5$. The buckling amplitude is obtained from equation (6) by substituting wavenumber k with $2\pi/\lambda_{\rm SWNT}$ as

$$(w_{\max})_{\rm SWNT} = \frac{14}{5}\left(\frac{\pi E_{\rm CNT}tR^3}{\bar{E}_{\rm S}}\right)^{1/4}\sqrt{\varepsilon_{\rm pre} - (\varepsilon_{\rm c})_{\rm SWNT}}$$
$$= \frac{\lambda_{\rm SWNT}}{\pi}\sqrt{\varepsilon_{\rm pre} - (\varepsilon_{\rm c})_{\rm SWNT}}, \qquad (12)$$

which is also linearly proportional to the buckling wavelength, and increases with the prestrain, where the critical buckling strain $(\varepsilon_{\rm c})_{\rm SWNT} = \alpha\{1 + 4\pi[5 - 2\gamma - 2\ln(5/7) - \ln\alpha]^{-1}\}/4$, and $\alpha = \sqrt{\bar{E}_{\rm S}R/(\pi E_{\rm CNT}t)}$. The amplitude is shown in figure 3(b) for the prestrain $\varepsilon_{\rm pre} = 5\%$.

The maximum strain in SWNT is the sum of membrane strain $\varepsilon_{\rm m} = k^2w_{\max}^2/4 - \varepsilon_{\rm pre} = -(\varepsilon_{\rm c})_{\rm SWNT}$ and bending strain $\varepsilon_{\rm b} = (\mathrm{d}^2w/\mathrm{d}x^2)R = -(10/7)[\bar{E}_{\rm S}R/(\pi E_{\rm CNT}t)]^{\frac{1}{4}}\sqrt{\varepsilon_{\rm pre} - (\varepsilon_{\rm c})_{\rm SWNT}}$. Its magnitude is

$$\varepsilon_{\max} = (\varepsilon_{\rm c})_{\rm SWNT} + \frac{10}{7}\left(\frac{\bar{E}_{\rm S}R}{\pi E_{\rm CNT}t}\right)^{\frac{1}{4}}\sqrt{\varepsilon_{\rm pre} - (\varepsilon_{\rm c})_{\rm SWNT}}$$
$$\approx \frac{10}{7}\left(\frac{\bar{E}_{\rm S}R}{\pi E_{\rm CNT}t}\right)^{\frac{1}{4}}\sqrt{\varepsilon_{\rm pre}}, \qquad (13)$$

where the critical buckling strain $(\varepsilon_{\rm c})_{\rm SWNT}$ is only 0.06% for the (10, 10) SWNT on PDMS. For $\varepsilon_{\rm pre} = 5\%$, 10% and 27%, the maximum strain in SWNT is 1.1%, 1.6% and 2.6%, respectively.

For $\varepsilon_{\rm pre} = 5\%$, as in the experiments of SWNT buckling on PDMS substrate [14], figure 3(c) shows that the potential energy for normal buckling is larger than that in equation (4) for in-surface buckling. However, their difference is much smaller than the adhesion energy (energy per unit length) between SWNTs and PDMS. The surface roughness of PDMS is comparable to or even larger than the SWNT radius (~1 nm), thereby giving rise to the possibility that this roughness can prevent the in-surface buckling mode [25].

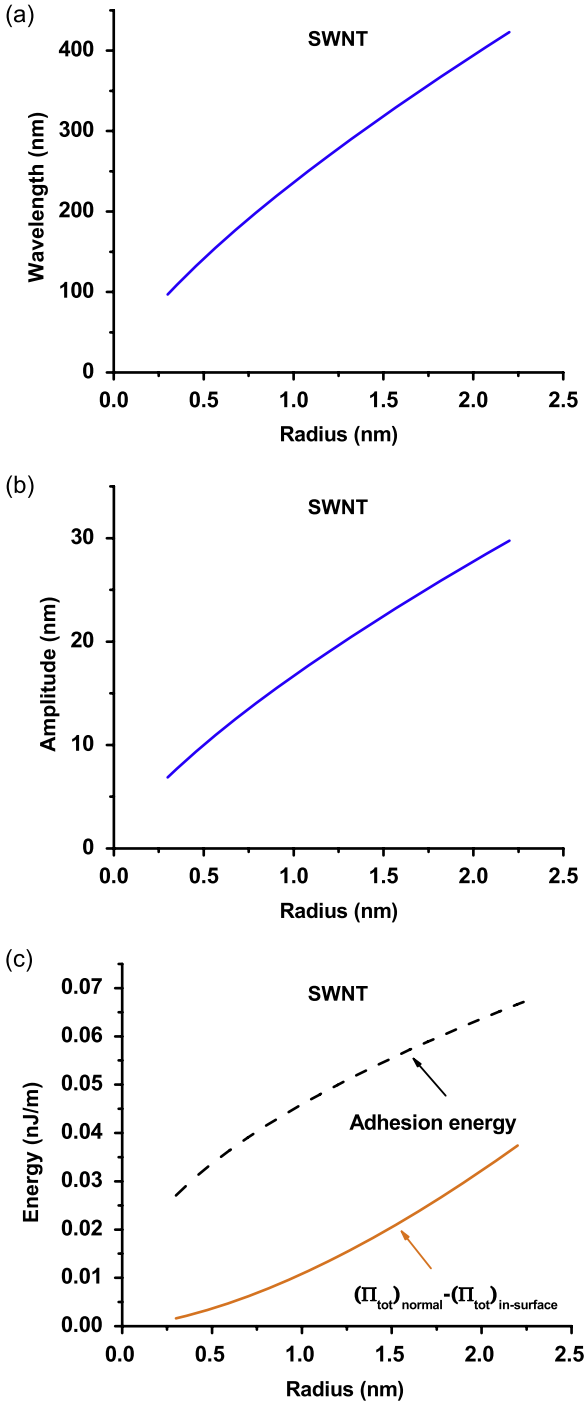

Figure 3. In-surface buckling of SWNTs on PDMS substrates. (a) Buckling wavelength versus SWNT radius. (b) Buckling amplitude versus SWNT radius. (c) Energy difference between normal and in-surface buckling, and the adhesion energy between SWNTs and PDMS, versus SWNT radius.

5. In-surface buckling of multi-walled carbon nanotubes on a PDMS substrate

For a n-wall MWNT with innermost wall radius $R_{\rm in}$ and inter-wall spacing $\sigma = 0.34$ nm, its bending stiffness and tension stiffness are $(E_{\rm CNT}I)_{\rm multi} = \pi E_{\rm CNT}tR_{\rm in}^3 n[1 + 3(n-1)\sigma/(2R_{\rm in}) + (n-1)(2n-1)\sigma^2/(2R_{\rm in}^2) + n(n-1)^2\sigma^3/(4R_{\rm in}^3)]$

and $(E_{\rm CNT}A)_{\rm multi} = 2\pi E_{\rm CNT}tR_{\rm in}n[1+(n-1)\sigma/(2R_{\rm in})]$, respectively [20]. The width $2w$ of the contact region between MWNT and substrate is $2R_{\rm out}$, where $R_{\rm out} = R_{\rm in}+(n-1)\sigma$ is the outermost wall radius. The wavelength of buckled MWNTs is obtained from equation (7) by substituting the bending stiffness EI with $(E_{\rm CNT}I)_{\rm multi}$ for MWNTs, and is given by

$$\lambda_{\rm MWNT} = \frac{14\pi}{5}\left[\frac{(E_{\rm CNT}I)_{\rm multi}}{\bar{E}_{\rm S}}\right]^{1/4}. \qquad (14)$$

The wavelength is shown versus the number of walls n by dots in figure 4(a) for (10, 10) SWNT ($R_{\rm in} = 0.69$ nm) as the innermost wall, $E_{\rm CNT}t = 0.42$ TPa nm, $E_{\rm S} = 2$ MPa, and $\nu_{\rm S} = 0.5$. For $n \gg 1$, the wavelength becomes $\lambda_{\rm MWNT} \approx (7\pi/5)[\pi E_{\rm CNT}t\sigma^3/(4\bar{E}_{\rm S})]^{1/4}(2n-1+2R_{\rm in}/\sigma)$, which increases linearly with the number of walls, and agrees well with the solution in figure 4(a). This linear relation results from the wavelength in equation (14) scaling with $(E_{\rm CNT}I)^{1/4}_{\rm multi}$ and the bending stiffness $(E_{\rm CNT}I)_{\rm multi}$ scaling with n^4 for large n.

The buckling amplitude of MWNTs is obtained from equation (6) by substituting wavenumber k with $2\pi/\lambda_{\rm MWNT}$ as

$$(v_{\rm max})_{\rm MWNT} = \frac{14}{5}\left[\frac{(E_{\rm CNT}I)_{\rm multi}}{\bar{E}_{\rm S}}\right]^{1/4}\sqrt{\varepsilon_{\rm pre}-(\varepsilon_{\rm c})_{\rm MWNT}} = \frac{\lambda_{\rm MWNT}}{\pi}\sqrt{\varepsilon_{\rm pre}-(\varepsilon_{\rm c})_{\rm MWNT}}, \qquad (15)$$

where the critical buckling strain $(\varepsilon_{\rm c})_{\rm MWNT} = \alpha^{(1)}_{\rm multi}\{1+4\pi[5-2\gamma-2\ln(5/7)-\ln\alpha^{(2)}_{\rm multi}]^{-1}\}/2$, $\alpha^{(1)}_{\rm multi} = \sqrt{\bar{E}_{\rm S}(E_{\rm CNT}I)_{\rm multi}}/(E_{\rm CNT}A)_{\rm multi}$ and $\alpha^{(2)}_{\rm multi} = R^2_{\rm out}\sqrt{\bar{E}_{\rm S}/(E_{\rm CNT}I)_{\rm multi}}$. The critical buckling strain decreases as n increases, from 0.061% for $n = 1$ to 0.044% for $n \geqslant 4$. The amplitude is shown versus the number of walls n in figure 4(b) for the prestrain $\varepsilon_{\rm pre} = 5\%$. For $n \gg 1$, the amplitude becomes $v_{\rm max} \approx (7/5)[\pi E_{\rm CNT}t\sigma^3/(4\bar{E}_{\rm S})]^{1/4}(2n-1+2R_{\rm in}/\sigma)\sqrt{\varepsilon_{\rm pre}-\varepsilon_{\rm c}}$, which is also linear with n, and agrees well with the solution in figure 4(b). This linearity is because the buckling amplitude in equation (15) is linearly proportional to the buckling wavelength.

For prestrain $\varepsilon_{\rm pre} = 5\%$ and (10, 10) SWNT ($R_{\rm in} = 0.69$ nm) as the innermost wall, figure 4(c) shows that the potential energy for normal buckling of a MWNT is larger than that for in-surface buckling. Their difference is smaller than the adhesion energy (energy per unit length) between MWNTs and PDMS for the number of walls $n \leqslant 7$, and becomes larger than the adhesion energy for $n > 8$, as shown in figure 4(c). This is because van der Waals interaction is negligible for two atoms of distance larger than 1 nm, so only the outmost two walls of a MWNT have contributions to the adhesion energy. On the other hand, the energy difference between two buckling modes is proportional to the bending stiffness $(E_{\rm CNT}I)_{\rm multi}$ of the MWNT, which is proportional to the number of walls n to the 4th power. Therefore, when the number of walls n increases, the energy difference between normal and in-surface buckling increases much faster than the adhesion energy. Furthermore, diameters of MWNTs of large number of walls are significantly larger than the surface roughness of PDMS (∼1 nm), and observing in-surface buckling of MWNTs in experiment could be possible.

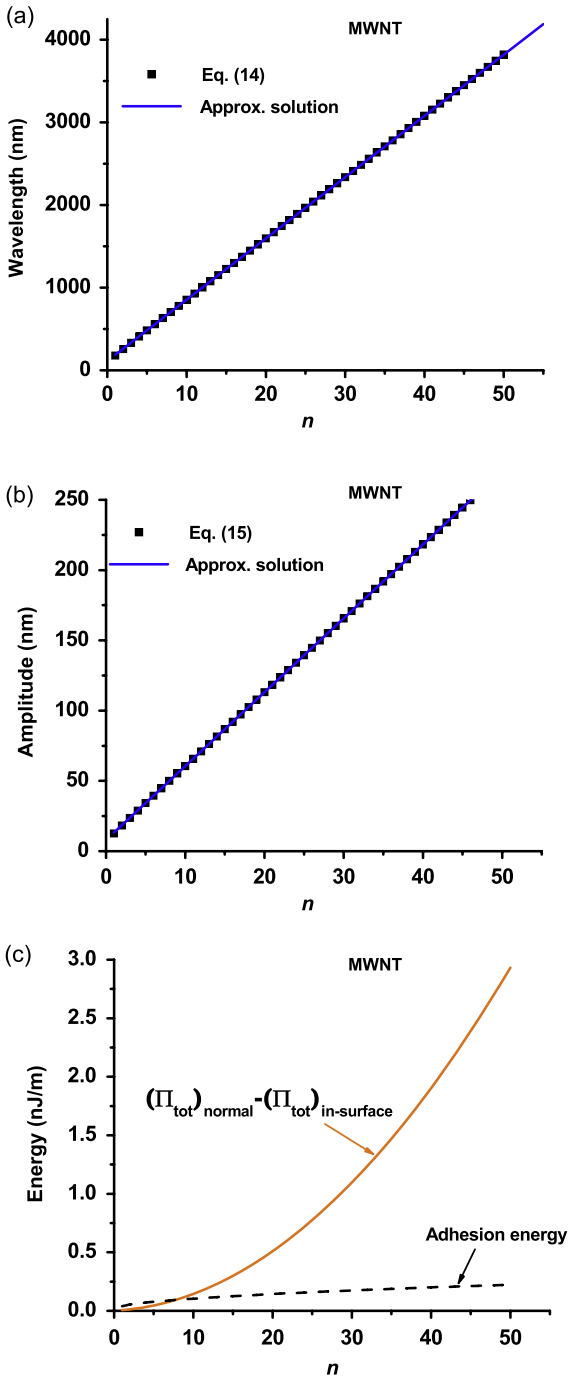

Figure 4. In-surface buckling of MWNTs on PDMS substrates. (a) Buckling wavelength versus number of walls. (b) Buckling amplitude versus number of walls. (c) Energy difference between normal and in-surface buckling, and the adhesion energy between MWNTs and PDMS, versus the number of walls of MWNTs.

6. In-surface buckling of carbon nanotube bundles on a PDMS substrate

A representative carbon nanotube bundle has 7 SWNTs of equal radius R forming a hexagon (one being at the center),

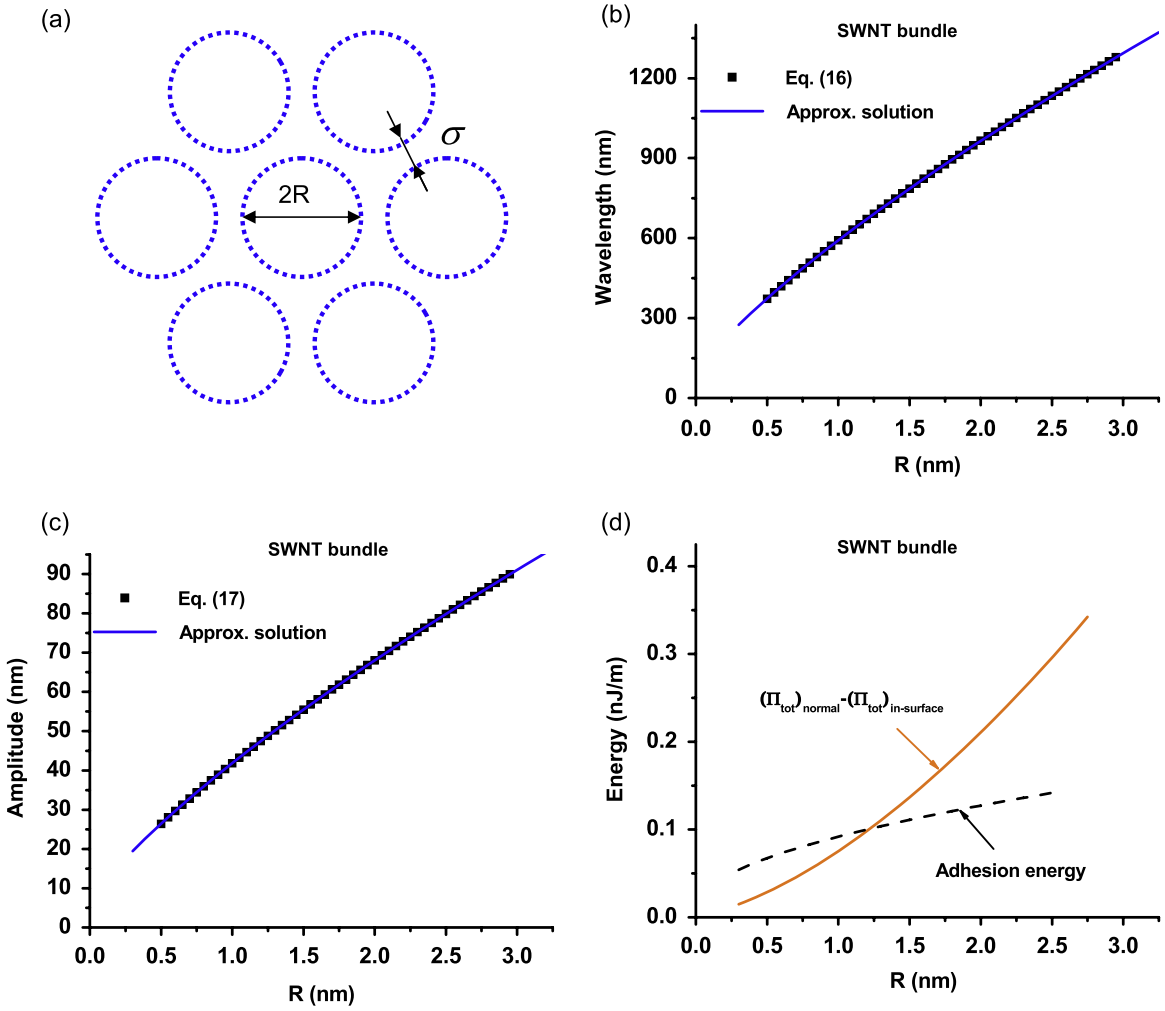

Figure 5. In-surface buckling of SWNT bundles on PDMS substrates. (a) Schematic illustration of a SWNT bundle. (b) Buckling wavelength versus SWNT radius. (c) Buckling amplitude versus SWNT radius. (d) Energy difference between normal and in-surface buckling, and the adhesion energy between SWNT bundles and PDMS, versus the constituent SWNT radius.

as shown in figure 5(a) [20]. The inter-tube spacing is $\sigma = 0.34$ nm. The bending stiffness and tension stiffness of the bundle are $(E_{\rm CNT}I)_{\rm bundle} = \pi E_{\rm CNT} t R^3[7 + 6(2 + \sigma/R)^2]$ and $(E_{\rm CNT}A)_{\rm bundle} = 14\pi E_{\rm CNT} t R$, respectively [20]. The width $2w$ of the contact region between the carbon nanotube bundles and the substrate is $2R_{\rm out}$, where $R_{\rm out} = 3R + \sigma$ is the outer radius of the bundle. The wavelength of carbon nanotube bundles is identical to that in equation (7) except that the bending stiffness EI is changed to $(E_{\rm CNT}I)_{\rm bundle}$,

$$\lambda_{\rm bundle} = \frac{14\pi}{5}\left[\frac{(E_{\rm CNT}I)_{\rm bundle}}{\bar{E}_{\rm S}}\right]^{1/4}. \qquad (16)$$

The wavelength is shown versus the SWNT radius R in figure 5(b), with $E_{\rm CNT}t = 0.42$ TPa nm, $E_{\rm S} = 2$ MPa, and $\nu_{\rm S} = 0.5$. For $R \gg \sigma$, the wavelength becomes $\lambda_{\rm bundle} \approx (14\pi/5)(31\pi E_{\rm CNT} t R^3/\bar{E}_{\rm S})^{1/4}[1 + 6\sigma/(31R)]$, which agrees well with the solution in figure 5(b).

The buckling amplitude of carbon nanotube bundles is obtained from equation (6) by substituting wavenumber k with $2\pi/\lambda_{\rm bundle}$ as

$$(\upsilon_{\max})_{\rm bundle} \approx \frac{14}{5}\left[\frac{(E_{\rm CNT}I)_{\rm bundle}}{\bar{E}_{\rm S}}\right]^{1/4}\sqrt{\varepsilon_{\rm pre} - (\varepsilon_{\rm c})_{\rm bundle}} = \frac{\lambda_{\rm bundle}}{\pi}\sqrt{\varepsilon_{\rm pre} - (\varepsilon_{\rm c})_{\rm bundle}}, \qquad (17)$$

where the critical buckling strain $(\varepsilon_{\rm c})_{\rm bundle} = \alpha^{(1)}_{\rm bundle}\{1 + 4\pi[5 - 2\gamma - 2\ln(5/7) - \ln\alpha^{(2)}_{\rm bundle}]^{-1}\}/2$, $\alpha^{(1)}_{\rm bundle} = \sqrt{\bar{E}_{\rm S}(E_{\rm CNT}I)_{\rm bundle}}/(E_{\rm CNT}A)_{\rm bundle}$ and $\alpha^{(2)}_{\rm bundle} = R^2_{\rm out}\sqrt{\bar{E}_{\rm S}/(E_{\rm CNT}I)_{\rm multi}}$. The critical buckling strain increases as R increases, from 0.05% for $R = 0.5$ nm to 0.09% for $R = 2.0$ nm. The amplitude is shown versus the SWNT radius R in figure 5(c) for the prestrain $\varepsilon_{\rm pre} = 5\%$. For $R \gg \sigma$, the amplitude becomes $\upsilon_{\max} \approx (14/5)(31\pi E_{\rm CNT} t R^3/\bar{E}_{\rm S})^{1/4}[1 + 6\sigma/(31R)]\sqrt{\varepsilon_{\rm pre} - \varepsilon_{\rm c}}$, which agrees well with the solution in figure 5(c).

Figure 5(d) shows that the potential energy for normal buckling of a SWNT bundle is also larger than that for in-surface buckling. For prestrain $\varepsilon_{\rm pre} = 5\%$, their difference is smaller than the adhesion energy (per unit length) between the SWNT bundle and PDMS when the tube radius $R < 1.3$ nm,

and is larger than the adhesion energy when tube radius $R >$ 1.3 nm. This is due to only the bottom two tubes of the bundle contributing to the adhesion energy.

7. Conclusions

A continuum mechanics theory is established to study in-surface buckling of stiff beams on elastomeric substrates. Simple analytical expressions are obtained for the buckling wavelength, amplitude and critical buckling strain. The theory is applied to in-surface buckling of SiNWs, SWNTs, MWNTs and carbon nanotube bundles on PDMS substrates. For SiNWs, the buckling wavelength increases linearly with the radius. The measured wavelength gives Young's modulus for SiNW $E_{\mathrm{SiNW}} = 140$ GPa, which agrees well with prior values reported for SiNW. For SWNTs or carbon nanotube bundles, the in-surface buckling wavelength is proportional respectively to the SWNT radius or radius of carbon nanotubes in the bundle to the 3/4 power. For MWNTs, the in-surface buckling wavelength increases linearly with the number of walls.

The energy for in-surface buckling is lower than that for normal (out-of-surface) buckling, and is therefore energetically favorable. The reason that only normal buckling of SWNTs is observed in a previous experiment [14] is due to the rather small energy difference between normal and in-surface buckling of SWNTs and the rather small SWNT diameter ($\sim$1 nm). For large MWNTs and SWNT bundles, it is possible to observe in-surface buckling behavior in experiment.

Acknowledgments

The authors acknowledge the support from the National Science Foundation (DMI-0328162, ECCS-0824129), NSFC, and National Research Foundation of Korea (NRF) through a grant (K2070400000307A050000310, Global Research Laboratory (GRL) Program) provided by the Korean Ministry of Education, Science & Technology (MEST) in 2009.

References

[1] Lacour S P, Wagner S, Huang Z Y and Suo Z 2003 *Appl. Phys. Lett.* **82** 2404–6
[2] Sun Y and Rogers J A 2007 *J. Mater. Chem.* **17** 832
[3] Lumelsky V J, Shur M S and Wagner S 2001 *IEEE Sensors J.* **1** 41
[4] Sun Y, Choi W M, Jiang H, Huang Y Y and Rogers J A 2006 *Nat. Nanotechnol.* **1** 201
[5] Khang D Y, Jiang H, Huang Y and Rogers J A 2006 *Science* **311** 208
[6] Sun Y, Kumar V, Adesida I and Rogers J A 2006 *Adv. Mater.* **18** 2857
[7] Lacour S P, Jones J, Wagner S, Li T and Suo Z 2005 *Proc. IEEE* **93** 1459
[8] Lacour S P, Jones J, Suo Z and Wagner S 2004 *IEEE Electron Device Lett.* **25** 179–81
[9] Bowden N, Brittain S, Evans A G, Hutchinson J W and Whitesides G M 1998 *Nature* **393** 146–9
[10] Choi W M, Song J, Khang D Y, Jiang H, Huang Y Y and Rogers J A 2007 *Nano Lett.* **7** 1655–63
[11] Kim D H, Song J, Choi W M, Kim H S, Kim R H, Liu Z, Huang Y Y, Hwang K C, Zhang Y W and Rogers J A 2008 *Proc. Natl Acad. Sci. USA* **105** 18675–80
[12] Stafford C M, Harrison C, Beers K L, Karim A, Amis E J, VanLandingham M R, Kim H C, Volksen W, Miller R D and Simonyi E E 2004 *Nat. Mater.* **3** 545
[13] Nolte A J, Rubner M F and Cohen R E 2005 *Macromolecules* **38** 5367
[14] Khang D Y, Xiao J, Kocabas C, Maclaren S, Banks T, Jiang H, Huang Y Y and Rogers J A 2008 *Nano Lett.* **8** 124–30
[15] Ko H C *et al* 2008 *Nature* **454** 748–53
[16] Huang Z Y, Hong W and Suo Z 2005 *J. Mech. Phys. Solids* **53** 2101–18
[17] Huang R and Suo Z 2002 *J. Appl. Phys.* **91** 1135–42
[18] Huang R and Suo Z 2002 *Int. J. Solids Struct.* **39** 1791–802
[19] Jiang H, Khang D Y, Fei H, Kim H, Huang Y, Xiao J and Rogers J A 2008 *J. Mech. Phys. Solids* **56** 2585–98
[20] Xiao J, Jiang H, Khang D Y, Wu J, Huang Y and Rogers J A 2008 *J. Appl. Phys.* **104** 033543
[21] Jiang H, Khang D Y, Song J, Sun Y G, Huang Y and Rogers J A 2007 *Proc. Natl Acad. Sci. USA* **104** 15607–12
[22] Jiang H, Sun Y, Rogers J A and Huang Y Y 2007 *Appl. Phys. Lett.* **90** 133119
[23] Song J, Huang Y, Xiao J, Wang S, Hwang K C, Ko H C, Kim D H, Stoykovich M P and Rogers J A 2009 *J. Appl. Phys.* **105** 123516
[24] Song J, Jiang H, Choi W M, Khang D Y, Huang Y and Rogers J A 2008 *J. Appl. Phys.* **103** 014303
[25] Ryu S Y, Xiao J, Park W I, Son K S, Huang Y Y, Paik U and Rogers J A 2009 *Nano Lett.* **9** 3214–9
[26] Cui Y, Lauhon L J, Gudiksen M S, Wang J and Lieber C M 2001 *Appl. Phys. Lett.* **78** 2214–6
[27] Hochbaum A I, Fan R, He R and Yang P 2005 *Nano Lett.* **5** 457–60
[28] Fan Z, Ho J C, Jacobson Z A, Yerushalmi R L, Alley R L, Razavi H and Javey A 2008 *Nano Lett.* **8** 20–5
[29] Meitl M A, Zhu Z T, Kumar V, Lee K J, Feng X, Huang Y Y, Adesida I, Nuzzo R G and Rogers J A 2006 *Nat. Mater.* **5** 33–8
[30] Huang Y Y, Zhou W, Hsia K J, Menard E, Park J U, Rogers J A and Alleyne A G 2005 *Langmuir* **21** 8058–68
[31] Zhou W, Huang Y, Menard E, Aluru N R, Rogers J A and Alleyne A G 2005 *Appl. Phys. Lett.* **87** 251925
[32] Feng X, Meitl M A, Bowen A M, Huang Y, Nuzzo R G and Rogers J A 2007 *Langmuir* **23** 12555–60
[33] Wang S, Song J, Kim D H, Huang Y and Rogers J A 2008 *Appl. Phys. Lett.* **93** 023126
[34] Zhang P, Jiang H, Huang Y, Geubelle P H and Hwang K C 2004 *J. Mech. Phys. Solids* **52** 977–98
[35] Zhang P, Huang Y, Geubelle P H, Klein P A and Hwang K C 2002 *Int. J. Solids Struct.* **39** 3893–906
[36] Kocabas C, Kim H S, Banks T, Rogers J A, Pesetski A A, Baumgardner J E, Krishnaswamy S V and Zhang H 2008 *Proc. Natl Acad. Sci. USA* **105** 1405–9
[37] Cao Q, Kim H S, Pimparkar N, Kulkarni J P, Wang C, Shim M, Roy K, Alam M A and Rogers J A 2008 *Nature* **454** 495–500
[38] Cui Y and Lieber C M 2001 *Science* **291** 851–3
[39] Cui Y, Zhong Z, Wang D, Wang W U and Lieber C M 2003 *Nano Lett.* **3** 149–52
[40] Jiang H, Liu B, Huang Y and Hwang K C 2004 *Trans. ASME, J. Eng. Mater. Technol.* **126** 265–70
[41] Liu B, Jiang H, Johnson H T and Huang Y 2004 *J. Mech. Phys. Solids* **52** 1–26
[42] Jiang H, Feng X Q, Huang Y, Hwang K C and Wu P D 2004 *Comput. Methods Appl. Mech. Eng.* **193** 3419–29
[43] Li D, Wu Y, Kim P and Shi L 2003 *Appl. Phys. Lett.* **83** 2934
[44] Song J, Wang X, Riedo E and Wang Z L 2005 *Nano Lett.* **5** 1954–8

[45] Lew K K, Pan L, Bogart T E, Dilts S M, Dickey E C, Redwing J M, Wang Y, Cabassi M, Mayer T S and Novak S W 2004 *Appl. Phys. Lett.* **85** 3101
[46] Choi K M and Rogers J A 2003 *J. Am. Chem. Soc.* **125** 4060–1
[47] Timoshenko S P 1956 *Strength of Materials* (New York: Van Nostrand)
[48] Saada A S 1993 *Elasticity: Theory and Applications* (Malabar, FL: Krieger)
[49] Abramowitz M and Stegun I A 1972 *Handbook of Mathematical Functions with Formulas, Graphs, and Mathematical Tables* (New York: Dover)
[50] Wu Y, Cui Y, Huynh L, Barrelet C J, Bell D C and Lieber C M 2004 *Nano Lett.* **4** 433–6
[51] Menon M, Srivastava D, Ponomareva I and Chernozatonskii L A 2004 *Phys. Rev.* B **70** 125313
[52] Li Q, Koo S M, Edelstein M D, Suehle J S and Richter C A 2007 *Nanotechnology* **18** 315202
[53] Hsin C L, Mai W, Gu Y, Gao Y, Huang C T, Liu Y, Chen L J and Wang Z L 2008 *Adv. Mater.* **20** 1–5
[54] Hoffmann S, Utke I, Moser B, Michler J, Christiansen S H, Schmidt V, Senz S, Werner P, Gösele U and Ballif C 2006 *Nano Lett.* **6** 622–5